MATERIALS SCIENCE

Hydrophilic directional slippery rough surfaces for water harvesting

Xianming Dai,[1,2]* Nan Sun,[1] Steven O. Nielsen,[3] Birgitt Boschitsch Stogin,[1] Jing Wang,[1] Shikuan Yang,[1] Tak-Sing Wong[1]*

Multifunctional surfaces that are favorable for both droplet nucleation and removal are highly desirable for water harvesting applications but are rare. Inspired by the unique functions of pitcher plants and rice leaves, we present a hydrophilic directional slippery rough surface (SRS) that is capable of rapidly nucleating and removing water droplets. Our surfaces consist of nanotextured directional microgrooves in which the nanotextures alone are infused with hydrophilic liquid lubricant. We have shown through molecular dynamics simulations that the physical origin of the efficient droplet nucleation is attributed to the hydrophilic surface functional groups, whereas the rapid droplet removal is due to the significantly reduced droplet pinning of the directional surface structures and slippery interface. We have further demonstrated that the SRS, owing to its large surface area, hydrophilic slippery interface, and directional liquid repellency, outperforms conventional liquid-repellent surfaces in water harvesting applications.

INTRODUCTION

Engineered surfaces with exceptional droplet nucleation and removal (*1*–*5*) are of great interest in various energy and water applications, including power generation (*6*), thermal management (*3*, *7*, *8*), water harvesting (*2*), and desalination (*9*). However, surfaces that have both exceptional droplet nucleation and removal capabilities are rare. For example, lotus leaf–inspired superhydrophobic surface(s) (SHS) (*10*–*12*) can effectively repel water droplets through air-infused surface textures and hydrophobic surface chemistry, but the trapped air can be easily damaged under pressure or high-humidity conditions. Once the trapped air is damaged, the liquids will be in full contact with the surface textures and become highly pinned (*13*, *14*), that is, the droplets will be in the Wenzel state (*15*). Advanced SHS designs have shown that it is possible to revert the Wenzel state droplets through the jumping droplet departure mechanism (*14*, *16*, *17*). Under a large subcooling condition, however, the formation of Wenzel state droplets becomes unavoidable because droplets nucleate within the surface textures. This greatly reduces droplet mobility and leads to surface flooding (*16*).

As an alternative strategy to resolve the droplet mobility issue of the SHS, new types of liquid-repellent surfaces modeled after the slippery rim of the *Nepenthes* pitcher plant have been developed. These surfaces, known as slippery liquid-infused porous surface(s) (SLIPS) (*18*, *19*), are characterized by a homogeneous and molecularly smooth interface made by fully infusing a textured surface with a hydrophobic liquid lubricant. These surfaces exhibit excellent droplet removal capabilities but suffer from relatively small surface area for droplet nucleation (*7*, *8*, *20*).

It is energetically more favorable for water vapor and small water droplets to nucleate on hydrophilic surfaces compared to hydrophobic ones (*2*, *21*–*23*). The *Namib* desert beetle, for example, uses patterned hydrophilic surfaces to nucleate and capture tiny water droplets in air for their survival (*2*). An ideal surface that sustains efficient droplet nucleation and removal must use hydrophilic surface chemistry and enhanced surface area to maximize droplet nucleation density, as well as must have a pinning-free slippery interface to enhance droplet mobility.

Here, we report the design and applications of a bioinspired slippery rough surface(s) (SRS), which combines the salient features of pitcher plants and rice leaves; our surface has hydrophilic surface chemistry, a slippery interface, directional structures, and large surface areas to maximize droplet collection and mobility (Fig. 1). Specifically, our SRS consists of liquid-infused nanotextures on directional microgrooves for enhanced droplet nucleation and transport. The presence of the nanoscale textures on the microgrooves helps retain a thin layer of hydrophilic lubricant to provide a slippery interface for droplet removal. Unlike the beetle-inspired surfaces where droplet nucleation only occurs in the patterned hydrophilic areas (*22*, *23*), our surfaces fully use the total surface area for maximized droplet nucleation. Such a surface allows nucleated droplets in the Wenzel state to be removed rapidly, which cannot be achieved by conventional rough surfaces. Here, we have demonstrated that the hydrophilic directional SRS outperforms many of the state-of-the art hydrophobic liquid-repellent surfaces such as SHS and SLIPS in dropwise condensation and fog harvesting owing to the large droplet nucleation density, and fast droplet coalescence and removal.

RESULTS

Design rationale I: Surface chemistry

The hydrophilic directional SRS involves a careful design of both surface wettability and structures. Surface wettability on a perfectly flat, rigid, and chemically homogeneous solid surface is governed by Young's equation: $\cos\theta_0 = \frac{\gamma_{SG}-\gamma_{SW}}{\gamma_{WG}}$, where γ_{SG} is the solid-gas interfacial tension, γ_{SW} is the solid-water interfacial tension, γ_{WG} is the water-gas interfacial tension, and θ_0 is the contact angle (CA) of the droplet on the smooth surface (Fig. 2A). This equation predicts the thermodynamically most stable CA on a smooth solid surface with negligible CA hysteresis. By infusing a liquid lubricant into a nanotextured surface, the liquid overcoat forms a homogeneous smooth surface (figs. S1 and S2) (*18*, *19*). Thus, the Young's equation can be modified to $\cos\theta = \frac{\gamma_{OG}-\gamma_{OW}}{\gamma_{WG}}$, where θ is the apparent CA of a water droplet on the liquid-infused substrate,

[1]Department of Mechanical and Nuclear Engineering and Materials Research Institute, Pennsylvania State University, University Park, PA 16802, USA. [2]Department of Mechanical Engineering, University of Texas at Dallas, Richardson, TX 75080, USA. [3]Department of Chemistry and Biochemistry, University of Texas at Dallas, Richardson, TX 75080, USA.
*Corresponding author. Email: dai@utdallas.edu (X.D.); tswong@psu.edu (T.-S.W.)

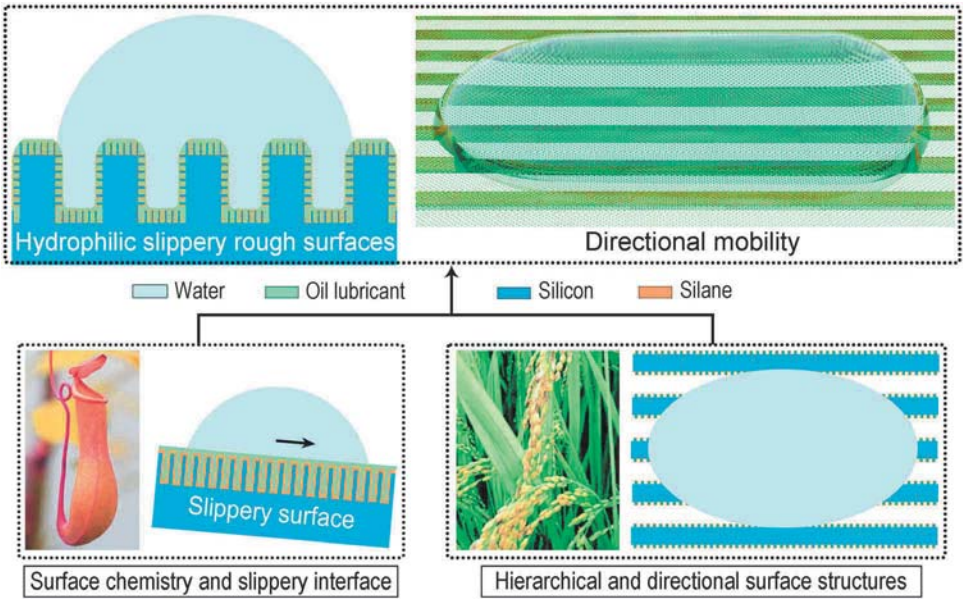

Fig. 1. Hydrophilic directional SRS inspired by pitcher plants and rice leaves. Side view (**top left**) and three-dimensional view (**top right**) of the hydrophilic directional SRS. Photos and schematics showing the pitcher plant–inspired slippery surface (**bottom left**) and rice leaf–inspired directional structured surface (**bottom right**). The photography of rice leaf was reprinted with permission from Bixler and Bhushan (*39*).

γ_{OG} is the lubricant-gas interfacial tension, γ_{OW} is the lubricant-water interfacial tension, and γ_{WG} is the water-gas interfacial tension (Fig. 2B). In this modified equation, all the interfacial tensions can be experimentally determined directly. Here, we refer to a surface as "hydrophobic" when $\theta > 90°$ and "hydrophilic" when $\theta < 90°$. According to the modified Young's equation, creating a hydrophilic surface (that is, $\theta < 90°$) would require γ_{OG} to be greater than γ_{OW} (that is, $\gamma_{OG} > \gamma_{OW}$), whereas creating a hydrophobic surface would require γ_{OG} to be smaller than γ_{OW} (that is, $\gamma_{OG} < \gamma_{OW}$).

On the basis of these physical insights, we have investigated a range of lubricants that could provide either hydrophobic or hydrophilic properties. To create a stable liquid-infused substrate, three engineering criteria must be satisfied (*18*, *19*). First, the surfaces must allow the lubricant to stably wet and conformally adhere to the solid textures. Second, it must be energetically more favorable for the lubricants, rather than water, to wet the solid textures. Third, the lubricant and water must be immiscible. The design principle of such a slippery surface includes careful selection of silane coating and lubricant, as well as the design of surface structures (fig. S1). We have investigated a number of water-immiscible hydrophobic and hydrophilic lubricants, such as perfluorinated oils, hydrocarbons, silicone oils with different terminal functional groups, and ionic liquids. These lubricants can stably wet the nanotextured surfaces with either perfluorinated silanes or trimethylchlorosilane (Sigma-Aldrich). Note that, in our surfaces, the surface wettability is primarily governed by the lubricant, not the underlying silane coating. The lubricants were applied onto the silanized nanotextured surfaces by a spin-coating process to maintain a microscopically thin layer of lubricant (*24*, *25*). Then, we characterized the static, advancing, and receding CAs on these liquid-infused smooth surfaces using an automated goniometer (ramé-hart) at room conditions with a 5-μl water droplet and compared these measurements with the predictions from the modified Young's equation. Note that the measured apparent CAs of these macroscopic droplets are based on the best fitting of the droplet geometries, and no noticeable oil meniscus was observed near the edge of the droplets (Fig. 2, E and F) because of the thin lubricant layer, which is on the order of 1 μm (*26*). CA hysteresis ($\Delta\theta$), which is the difference between advancing (θ_A) and receding (θ_R) CAs, is used to characterize the degree of water droplet pinning onto the surface. The CA hysteresis for these surfaces is less than 5°. The negligible CA hysteresis indicates that pinning of water droplets on all of these lubricated surfaces is minimal (Fig. 2C).

The measured static CAs range from 121.5° for a hydrophobic SLIPS with perfluorinated lubricant down to 76.2° for a hydrophilic SLIPS with hydroxy-terminated polydimethylsiloxane (PDMS) as the lubricant (Fig. 2, D to F, and movie S1). Hydroxy-terminated PDMSs with a viscosity of 25, 65, and 95 cSt are referred to as hydroxy PDMS-25, PDMS-65, and PDMS-95, respectively. Our experimental measurements indicated that the modified Young's equation can precisely predict the apparent CAs for these lubricated smooth surfaces. Note that the applicability of the modified Young's equation is contingent on three criteria. First, the surface textures have to be fully immersed under the lubricant layer (figs. S2 and S3). Second, the lubricant thickness has to be significantly smaller than the height of the droplet. Relatively thick lubricants could lead to surface deformation, and the resulting CA will significantly deviate from the theoretical predictions. The typical thickness of the lubricant is on the same order of the height of the nanotextures (that is, ~1 to 2 μm; fig. S2). Third, if a thin lubricant wrapping layer around the water droplet exists, then the governing equation would need to be modified to account for the presence of the wrapping layer (that is, by replacing γ_{WG} with $\gamma_{OG} + \gamma_{OW}$ in the modified Young's equation). When these criteria are met, the experimental measurements on the macroscopic droplets are in excellent agreement with those predicted by the modified Young's equation (table S1). As a result, the modified Young's equation allows us to precisely engineer the wettability of the liquid-infused smooth surfaces, which can be achieved by using appropriate lubricants.

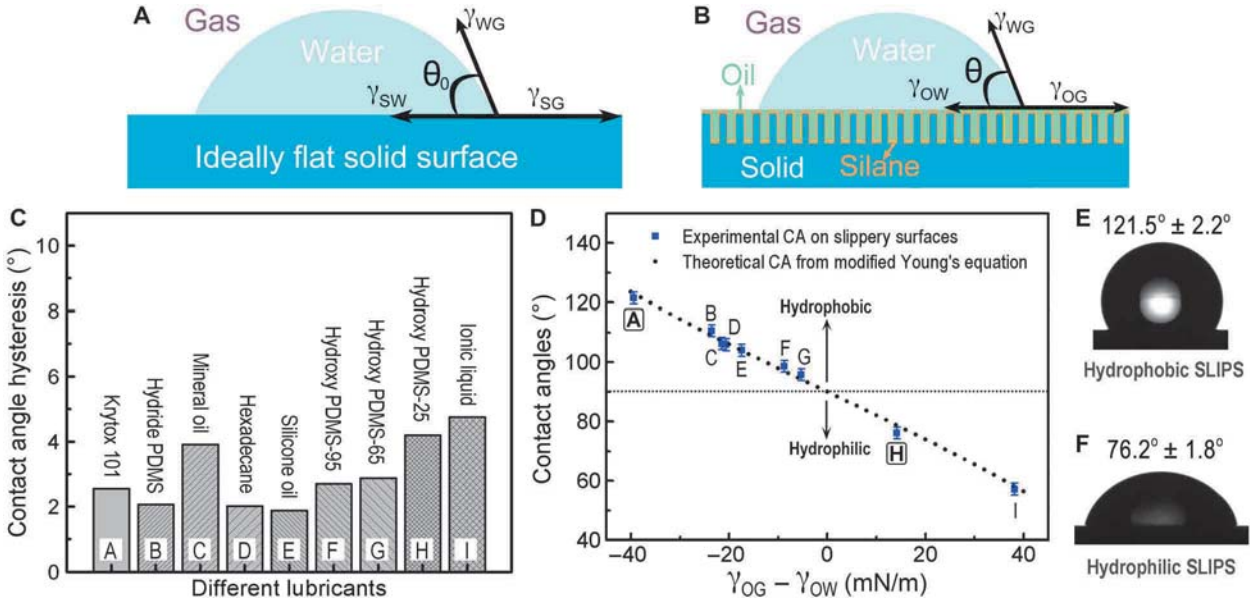

Fig. 2. Wetting characteristics of water droplets on lubricant-infused nanostructured surfaces. Schematic showing a liquid droplet sitting on a chemically homogeneous and smooth solid surface (**A**) and a SLIPS (**B**). (**C**) CA hysteresis of 5-μl water droplets on SLIPS with different lubricants. Note that ionic liquid used in the experiment is 1-butyl-3-methylimidazolium hexafluorophosphate ([bmim][PF_6]). (**D**) Comparison of theoretical prediction and experimental measurements of water CAs on hydrophobic and hydrophilic SLIPS. The capital letters correspond to the lubricants used (C). Note that, in our surfaces, the surface wettability is governed by the lubricant, not the underlying silane coating. Optical images showing a macroscopic water droplet on a hydrophobic (**E**) and a hydrophilic (**F**) SLIPS without any noticeable oil meniscus at the contact line. Krytox 101 and hydroxy PDMS-25 are used as our hydrophobic and hydrophilic lubricants, respectively.

Design rationale II: Surface structure

To design a surface for effective condensation, it is important to increase the number of potential nucleation sites (that is, surface area) without compromising the droplet mobility. Although SLIPS is known for its excellent droplet mobility, the molecularly smooth and flat surface leads to relatively low numbers of droplet nucleation events. To this end, we have designed three different SRS: lubricated micropillar arrays (isotropic SRS), lubricated microgrooves perpendicular to the droplet sliding direction (perpendicular SRS), and lubricated microgrooves parallel to the sliding direction (parallel SRS; fig. S5, A and B). Hydroxy PDMS-25 is used as the lubricant for all these surfaces. Note that the isotropic SRS and perpendicular/parallel SRS have the dimensions of width (50 μm), spacing (50 μm), and height (20 μm). The perpendicular and parallel SRS are the same sample but were placed at different orientations during the experiments. The surface roughness factor R (defined as the ratio of the apparent surface area and the projected surface area) of SLIPS and the SRS used in our experiments are ~1 and ~1.4, respectively.

We compared the droplet mobility on these three SRS with a SLIPS, which consists of liquid-infused nanotextures. Note that all the SRS are in full contact with the water droplets (that is, droplets are in the Wenzel state) in the experiments. Compared with the isotropic and perpendicular SRS, the parallel SRS has a smaller CA hysteresis (that is, 1.9° ± 0.8°) that is comparable to that on SLIPS (that is, 1.2° ± 0.5°; fig. S5A). This is due to small pinning effects on the liquid droplets in the direction parallel to the slippery microgrooves, a property that is consistent with the directional wetting of the rice leaves (*27*, *28*). Because the retention force for a liquid droplet on a surface is proportional to $\cos\theta_R - \cos\theta_A$ (*29*), liquid droplets condensed on the parallel SRS and SLIPS would experience similar retention forces. However, the augmented surface area of parallel SRS as compared to SLIPS will lead to a significantly increased number of nucleation events, which will further facilitate the droplet condensation and removal process. Overall, our results indicate that it is possible to design a surface with greatly enhanced surface area without compromising the droplet mobility when the droplets are in the Wenzel state, which is important for condensation and water harvesting purposes.

Dropwise condensation

Condensation is a phase change heat transfer process, where a vapor releases its latent heat and is converted into water droplets. We first investigated the influence of surface wettability on the condensation performances of the slippery smooth surfaces (that is, SLIPS). Dropwise condensation experiments were performed using an environmental scanning electronic microscope (ESEM). This allowed us to observe the droplet nucleation, coalescence dynamics, and mobility at the microscale. The samples were fixed at a tilt angle of 60° on a tilting stage. Then, we set the cooling temperature to –4.5° ± 0.5°C and the chamber pressure to 3.8 torr (where the associated saturation temperature is –2.5°C) to maintain the continuous condensation from vapor to water droplets. We visualized the droplet dynamics at the microscale on two different water-repellent surfaces, namely, (i) hydrophobic and (ii) hydrophilic SLIPS. The hydrophobic and hydrophilic SLIPS were composed of perfluorinated oil (θ = 121.5°) and hydroxy PDMS-25 (θ = 76.2°) lubricants, respectively.

Despite the effectiveness of the slippery surfaces in removing condensed droplets, we observed that hydrophobic SLIPS greatly hindered droplet nucleation during the condensation process compared to its hydrophilic counterpart (Fig. 3, A to D). For example, the visible droplet density (that is, the maximum number of droplets per unit area with the droplet size <14 μm) during the droplet nucleation process on hydrophilic SLIPS is ~268% higher than that on hydrophobic SLIPS at a

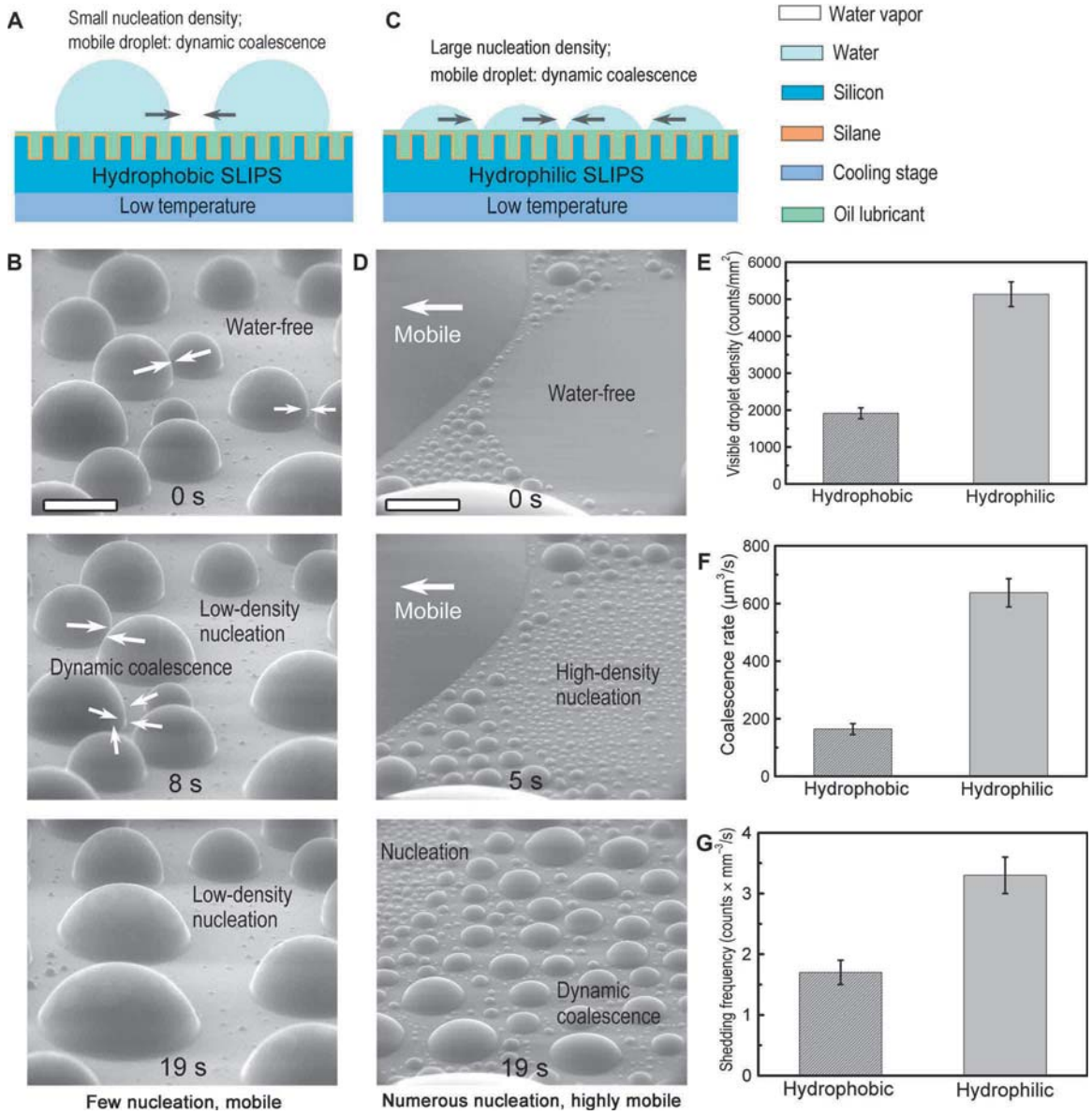

Fig. 3. Influence of surface chemistry on dropwise condensation performance. (**A**) Schematic showing dynamic coalescence on a hydrophobic slippery surface with small nucleation density. (**B**) Microscale condensate on a hydrophobic slippery surface (with Krytox 101 as the lubricant; CA = 121.5° ± 2.2°). The droplets are highly mobile, resulting in dynamic coalescence, but the hydrophobic nature of the surface limits droplet nucleation. (**C**) Schematic showing dynamic coalescence on a hydrophilic slippery surface. The surface has a large number of nucleation sites, resulting in efficient coalescence. The large contact area of the droplets facilitates heat conduction from the hot side to the cold side and coalescence of neighboring droplets. (**D**) Microscale condensate on a hydrophilic slippery surface. The surface has numerous nucleation sites, and the droplets are highly mobile (with hydroxy PDMS-25 as the lubricant; CA = 76.2° ± 1.8°). (**E**) Visible droplet density (that is, the maximum number of droplets per unit area with droplet size <14 μm during the nucleation process) on the hydrophilic and hydrophobic slippery surfaces. (**F**) Coalescence rate on the hydrophilic and hydrophobic slippery surfaces. (**G**) Shedding frequency of coalesced droplets on the hydrophilic and hydrophobic slippery surfaces. The tilt angle of the surface is 60°. Scale bars, 100 μm. Error bars represent SDs of measurements from three separate image analyses of a given condensation experiment.

temperature of −4.5° ± 0.5°C (Fig. 3, B, D, and E, and movie S2). This observation is consistent with a recent condensation theory, which predicts that hydrophilic substrates could lead to almost an order of magnitude higher droplet nucleation density compared to hydrophobic surfaces (*21*).

Fast droplet coalescence on hydrophilic slippery surfaces can effectively increase the droplet volume over time, which in turn favors fast droplet removal by gravity (Fig. 3, C and F). We calculated the coalescence rate by measuring the time from the onset of nucleation to the time the largest observed droplet reaches a specified volume (for example, ~4462 μm^3). The coalescence rate on the hydrophilic slippery surface is ~388% higher than that on the hydrophobic one. This finding can be understood from three perspectives: First, each single droplet on a hydrophilic surface has a larger contact area compared to the one with the same droplet volume on a hydrophobic surface. This reduces the effective distance between the neighboring droplets, which creates an environment that promotes the occurrence of coalescence events. Second, the relatively large nucleation density enables faster droplet coalescence

because the droplets are closer to each other on the hydrophilic surface. Finally, we have observed that microscale water droplets on some of the hydrophobic lubricants form a wrapping layer at the water-air interface, which leads to non-coalescence droplets, and greatly reduce the coalescence rate (*30*). However, these non-coalescence events have not been observed in the hydroxy PDMS system (movie S3), which could also account for the faster droplet coalescence rate for the hydrophilic SLIPS.

In addition to droplet coalescence, shedding of droplets by gravity is an important droplet removal mechanism during the condensation process. Here, the shedding of a droplet occurs when the gravity acting on a growing droplet overcomes the surface retention force (*29*). The shedding frequency of condensate droplets on the hydrophilic slippery surface is ~194% higher than that on the hydrophobic one (Fig. 3, D and G). Distinct from the vertical jumping droplet motion on SHS (*12*), the tangential sweeping droplet movement is another efficient mechanism for droplet coalescence and removal (*31*). On the hydrophilic slippery surfaces, droplet sweeping can occur efficiently owing to the high-density nucleation, resulting in fast removal of adjacent droplets. Note that this phenomenon has never been observed on hydrophilic solid surfaces previously because of the pinning of liquid droplets at defects and surface flooding.

Because the nucleation process originates at the molecular scale, experimental study of nucleation is extremely challenging. Therefore, we have performed molecular dynamics (MD) simulations to gain further physical insight into the nucleation process on our surfaces (Fig. 4). Building on recent MD studies showing the effect of surface energy (or surface wettability) on condensation nucleation (*32*), we considered the functional groups relevant to our surface chemistry displayed as the terminal groups on an alkanethiol self-assembled monolayer (SAM). Namely, we characterize the influence of different functional groups on nucleation by using a well-defined control surface. Our MD simulations demonstrate that surface functional groups can significantly influence the nucleation process on the liquid-infused surfaces. In our MD simulations, the SAM surface is kept at 373 K, whereas the initial water vapor temperature is set at 450 K. The nucleation rate for each functional group was characterized from an average of nine independent simulations as the time for most (70%) of the water vapor molecules to condense on the surface. Our data show that the more hydrophilic the surface, the faster the vapor condenses. For example, the –OH group showed ~16 and ~17 times faster heterogeneous nucleation rates than the $–CH_3$ and $–CF_3$ groups, respectively (Fig. 4E and table S2).

We observed that, on hydrophobic surfaces (that is, the $–CH_3$ and $–CF_3$ terminated SAMs), individual water molecules or small clusters that impact the surface will return to the vapor phase due to the relatively weak attraction forces (fig. S7), similar to those observed by Xu *et al.* (*32*). Only when a large enough cluster of around 50 ± 20 water molecules encounters the surface does it finally attach onto the surface, and at that point, the cluster continues to grow while maintaining a high CA (Fig. 4, A and B). In contrast, for a hydrophilic surface (that is, the –OH terminated SAM), individual water molecules or small clusters attach directly onto the surface without revisiting the bulk vapor phase (Fig. 4C); therefore, the formation of water clusters within the bulk vapor phase (which can be thought of as homogeneous nucleation) is suppressed. This greatly enhances the water condensation process on the surface. In addition, the growing water clusters spread on the surface, which is consistent with the wetting characteristic of a hydrophilic surface. This further enhanced the vapor condensation rate because there is a much larger surface area on the hydrophilic surface for water vapor to condense, whereas for the hydrophobic surfaces, the water vapor is restricted to condensing onto a small surface area because the droplet is prevented from spreading due to the surface hydrophobicity.

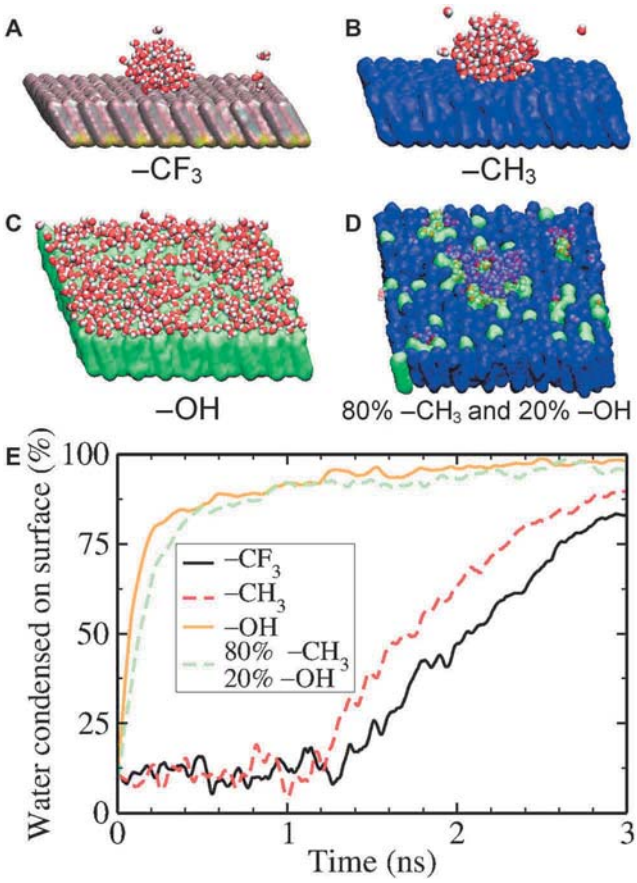

Fig. 4. MD simulations of water condensed on SAMs. Representative snapshots of water droplets/layers for (**A**) $–CF_3$ functional groups, (**B**) $–CH_3$ functional groups, (**C**) –OH functional groups, and (**D**) hydroxy PDMS (80% $–CH_3$ and 20% –OH functional groups). The CA during droplet growth is consistent with the macroscopic angle expected for each surface chemistry but with large fluctuations. (**E**) Water condensation timeline for a representative simulation of each surface chemistry in (A) to (D). The *y* axis records the number of water molecules within 4 nm (in the *z* direction) of the surface; this includes some vapor and thus has a nonzero baseline, as shown in the plot.

With this fundamental understanding, we constructed a model system to consider the nucleation process on hydroxy PDMS using MD simulations. On the basis of the composition of the hydroxy PDMS we used in our experiments, we constructed a SAM surface that consists of randomly distributed 80% $–CH_3$ and 20% –OH terminal functional groups. Water condensation occurs in the vicinity of the –OH sites, as shown in Fig. 4D and fig. S7. In particular, the nucleation rate on hydroxy PDMS is about seven and six times faster than that on the $–CF_3$ and $–CH_3$ terminated surfaces, respectively (Fig. 4E and table S2). These results are consistent with related MD studies showing that hydrophilic spots can have a large effect on the surface-water interactions (*2*, *33*, *34*). Our MD simulations provide the molecular basis on how a hydroxy-terminated surface can enhance the surface-water interactions, thereby significantly reducing the water nucleation time on the surface. This further supports the importance of hydrophilic surface chemistry in promoting water nucleation.

Next, we investigated the influence of a slippery interface (that is, liquid lubrication) on the overall dropwise condensation performance. We compared the performance of micro/nano hierarchical microgrooves (that is, hierarchical SHS) and hydrophilic parallel SRS (that is, hierarchical SHS with a conformally coated lubricant layer) to determine the influence of a slippery interface on condensation efficiency. Note that the hierarchical SHS used in this study do not perform jumping droplet function. Compared to hierarchical SHS (Fig. 5A), our hydrophilic parallel SRS have much higher droplet mobility due to slippery interfaces while the nucleated droplets on the SHS are highly pinned (Fig. 5, A and C, and movies S3 and S4). Liquid-infused slippery surfaces favor droplet growth and movement due to the higher thermal conductivity of oil than gas and negligible CA hysteresis (*8*, *35*). For example, the thermal conductivity of hydroxy PDMS-25 is ~0.15 W/(m·K), which is about six times higher than that of air (table S1). Thus, liquid lubricant could substantially reduce the thermal resistance for heat conduction compared to gas lubricant in SHS (Fig. 5A). In addition, a single microscale droplet can be highly mobile on the liquid lubricant, resulting in a more effective droplet coalescence and removal on liquid-infused surfaces compared to SHS, where the droplet is in contact with the solid surface. As shown by our ESEM studies, the SRS can remove condensates faster, quickly re-exposing large water-free regions for further condensation. This indicates that the presence of the lubricant layer greatly enhances droplet mobility and removal. Note that, to facilitate the droplet coalescence, it is desirable to use a thin lubricant layer (that is, on the order of 1 μm or less) because relatively thick lubricant layers [for example, >50 ± 10 μm; see the study of Boreyko *et al.* (*30*)] will be prone to the formation of droplets with significant wrapping layers and form non-coalescence droplets.

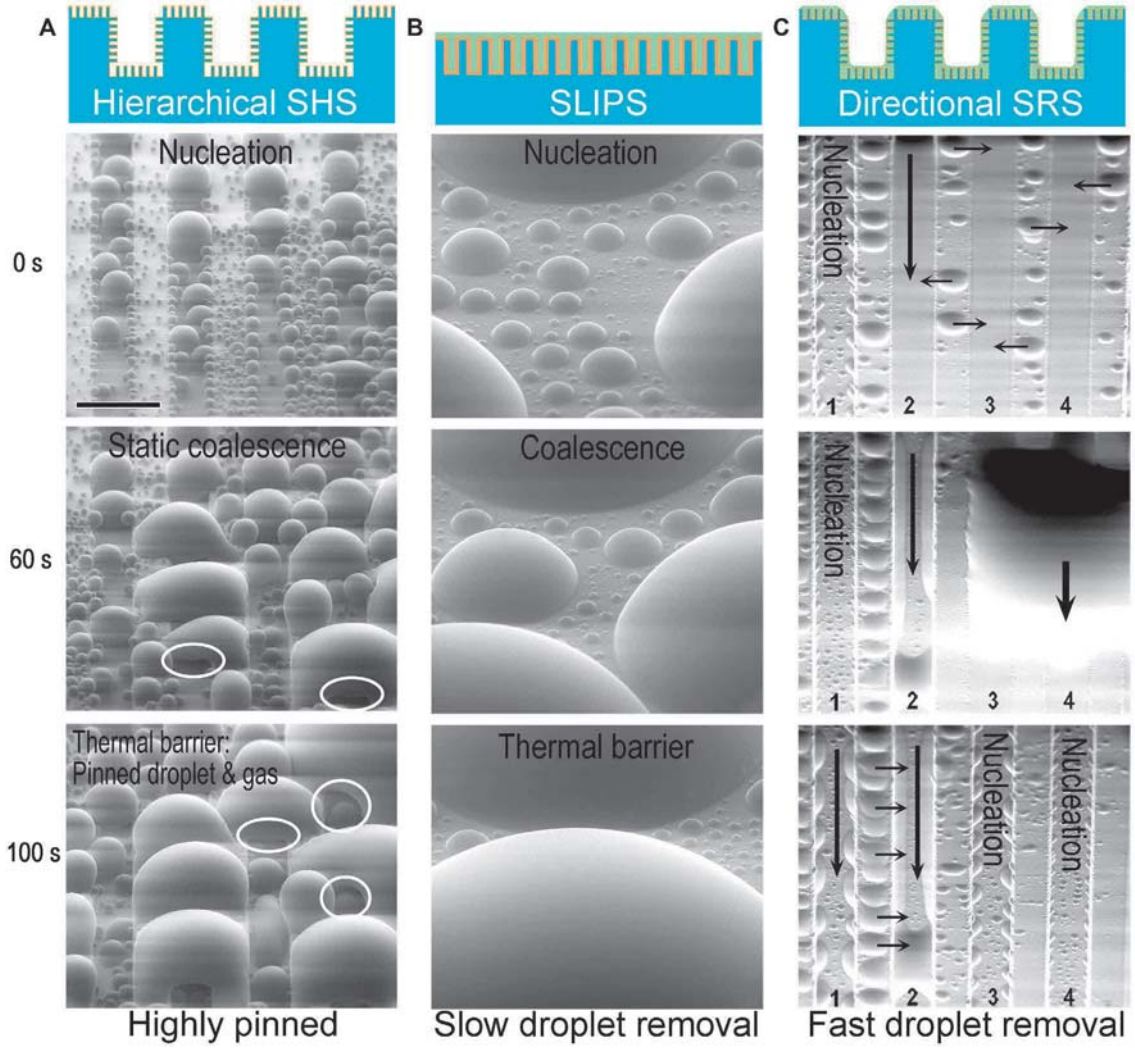

Fig. 5. Dropwise condensation on hierarchical SHS, hydrophilic SLIPS, and hydrophilic directional SRS. (**A**) Condensation on a hierarchical SHS. The droplets are highly pinned, and the SHS shows complete flooding after 100 s. The presence of gas holes (highlighted with white circles) acts as a thermal barrier and hinders heat transport. (**B**) Condensation on a hydrophilic SLIPS. Smaller droplets coalesce and are rapidly removed, but the larger droplets act as thermal barriers on the surface. (**C**) Condensation on a hydrophilic directional SRS. Smaller droplets move into the slippery microchannels, and larger droplets can be effectively drained away by the slippery microchannels. Hydroxy PDMS-25 was used on the SLIPS and on the SRS to ensure that they had the same surface chemistry. Note that the orientations of the SEM images in (C) were rotated 180° so that the direction of gravity in the image and in reality (for the reader) is aligned. The surface was tilted by 60° during the tests. Scale bar, 100 μm (for all images).

Finally, we compared the performance of hydrophilic SLIPS and hydrophilic parallel SRS to understand the effect of microscale structures and increased surface area. Compared to SLIPS, SRS have a larger exposed surface per unit projected area and therefore more nucleation sites. Furthermore, the capillary wetting and effective drainage on SRS resulted in faster condensate removal relative to SLIPS, leading to superior vapor condensation performance (Fig. 5, B and C, and movie S5). Overall, the hydrophilic parallel SRS showed a superior condensation performance over its equivalent hierarchical SHS and SLIPS owing to the significantly improved droplet nucleation, coalescence, and shedding.

Fog harvesting

In another application example, we used the hydrophilic parallel SRS for fog harvesting at the macroscale (Fig. 6). Fog harvesting is a water collection process where tiny water droplets from mist are adsorbed onto a surface without any heat transfer (*2*, *36*). In our measurements, we used an infrared camera and thermocouple to measure the surface, water, and atmosphere temperatures to ensure that there is no net temperature difference for the occurrence of heat transfer.

First, we investigated the influence of surface chemistry on the overall fog harvesting performance. When we compared the performance of hydrophobic and hydrophilic SLIPS (Fig. 6 and movie S6), we found that hydrophilic SLIPS exhibited a fog harvesting rate of 351.2 ± 9.2 mg/(hr·cm^2), which is 71.1 ± 4.4% higher than that of a hydrophobic SLIPS (Fig. 6D). The result further reinforces that it is energetically more favorable for tiny water droplets from the mist to adsorb onto hydrophilic slippery surfaces than onto the hydrophobic ones, and highlights the importance of the hydrophilic surface chemistry for fog

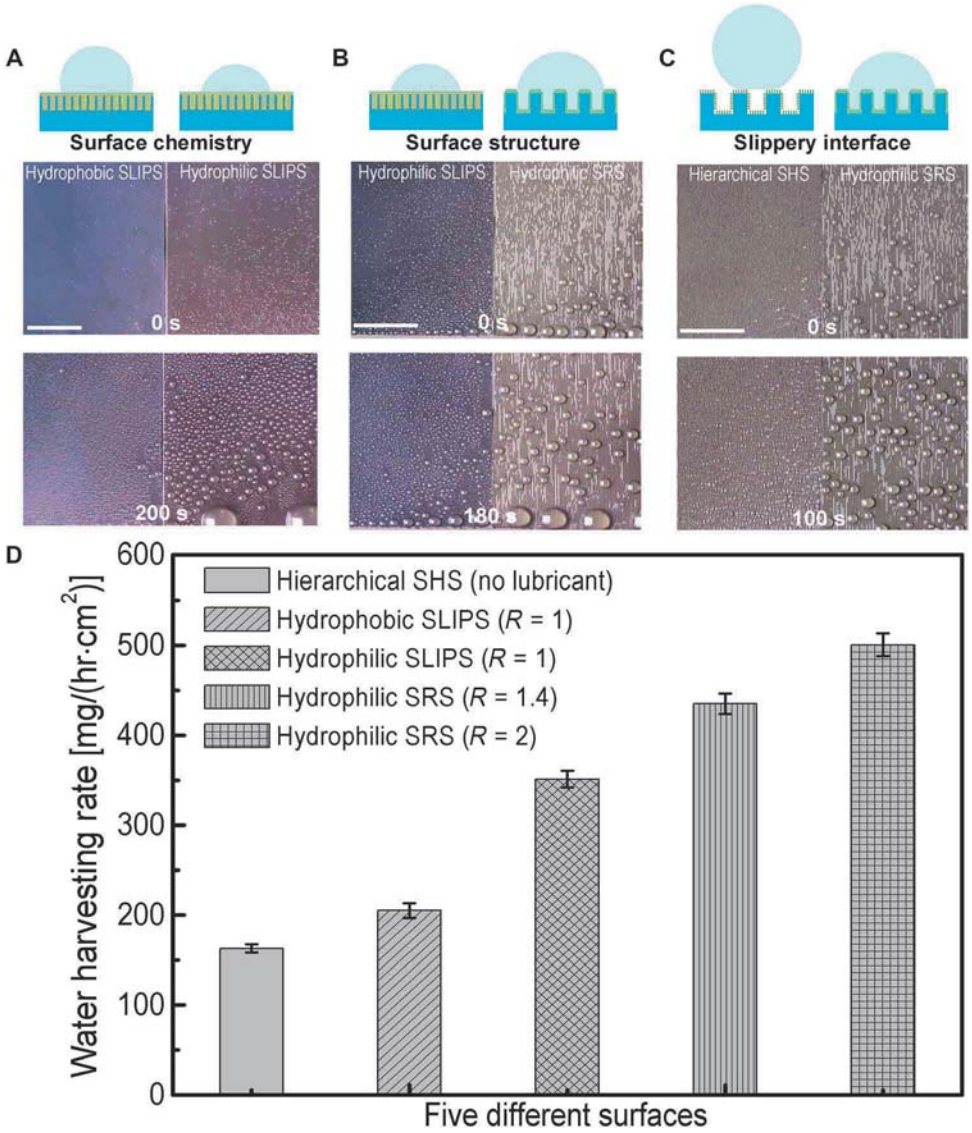

Fig. 6. Fog harvesting on hydrophobic SLIPS, hydrophilic SLIPS, hydrophilic SRS, and hierarchical SHS. Optical images showing water droplet nucleation and mobility comparisons for the following: (**A**) the influence of surface chemistry (fog harvesting on hydrophobic and hydrophilic SLIPS), (**B**) the influence of surface structure (fog harvesting on hydrophilic SLIPS and hydrophilic directional SRS), and (**C**) the influence of slippery interface (fog harvesting on hierarchical SHS and hydrophilic directional SRS). (**D**) Fog harvesting rates on different surfaces. The surfaces were positioned vertically during the tests. Scale bars, 5 mm. Error bars represent SDs from three individual measurements.

harvesting. In addition to hydrophobic and hydrophilic SLIPS, we have also compared the fog harvesting performances of hydrophilic SRS and hydrophobic SRS of R = ~2 (movie S7). On the hydrophilic SRS, droplets can be absorbed and transported away faster. This is due to the hydrophilic surface chemistry where the spreading of droplets favors droplet coalescence and removal. However, on the hydrophobic SRS, the water absorption is comparatively slower. Therefore, our direct experimental comparison shows that the hydrophilic SRS performs better in fog harvesting than hydrophobic SRS.

Next, we investigated the influence of a slippery interface on the fog harvesting performance. We compared the performance of hierarchical SHS and hydrophilic parallel SRS (Fig. 6B and movie S8). The channel and pillar widths for the parallel SRS were both 50 μm with a depth ranging from 20 to 50 μm, which corresponds to roughness factors of ~1.4 and ~2, respectively. The fog harvesting rate on the hydrophilic parallel SRS is 206.9 ± 7.7% better compared with the hierarchical parallel SHS (Fig. 6, C and D). The large air fraction of the nanoscale textures of SHS encourages tiny water droplets larger than the nanopillar spacing from attaching to the surface by maintaining them in the Cassie state (movie S8). When smaller water vapor droplets adhere onto the surface, they would enter the Wenzel state because of high Laplace pressure arising from the nanoscale spacing of the nanotextures and become pinned. As a result, hierarchical SHS displayed a much smaller droplet removal rate compared to that of hydrophilic parallel SRS. This observation is consistent with the fog harvesting performance on a control nanotexture-only SHS, where the performance is inferior to that of the hydrophilic SLIPS (that is, nanotextured SHS infused with the hydrophilic lubricant; movie S9).

Finally, we investigated the influence of surface structures on fog harvesting performance. We compared the performance of hydrophilic SLIPS and hydrophilic parallel SRS (Fig. 6, C and D). The hydrophilic parallel SRS (with the height h = 20 μm) exhibited a fog harvesting rate of 435.1 ± 11.3 mg/(hr·cm^2), which is 23.9 ± 3.2% better than hydrophilic SLIPS. The slippery microgrooves are favorable for droplet coalescence and efficient for water drainage, resulting in fast droplet removal (Fig. 6D and movie S10). By increasing the heights of the microgrooves from 20 to 50 μm at a constant width of 50 μm (that is, R increases from ~1.4 to ~2), the fog harvesting rate on parallel SRS can be further increased by 15.1 ± 2.9% (Fig. 6D). This indicates that the fog harvesting performance can be further enhanced by engineering the dimensions of the surface structures. We note that while increasing surface roughness enhances fog harvesting rates, the rate increase is not proportional to the surface area because the fog harvesting process is also dependent on the droplet coalescence and transport. Parametric study on the channel geometry of the directional SRS on the overall fog harvesting rate will be interesting to investigate further and will be a subject of future study.

Overall, the fog harvesting rate on the hydrophilic parallel SRS investigated here is 206.9 ± 7.7% and 143.8 ± 6.1% higher than that on the hierarchical SHS and hydrophobic SLIPS, respectively. Therefore, hydrophilic parallel SRS showed the best performance in fog harvesting compared to the hydrophilic and hydrophobic SLIPS, as well as the SHS present in this study.

DISCUSSION

In summary, we have demonstrated that hydrophilic directional SRS can outperform their hydrophobic counterparts and nonlubricated SHS in both droplet nucleation and mobility during dropwise condensation and fog harvesting processes. Many of these water condensates have traditionally pinned to the surface textures—a result of an irreversible transition from the Cassie state to the "sticky" Wenzel state. Our hydrophilic directional SRS resolves this long-standing issue by combining the unique surface functions of pitcher plants (that is, slippery interface) and rice leaves (that is, directional structures and micro/nano hierarchical structures), which can repel liquids regardless of how they wet the surfaces. Note that the longevity and robustness of the hydrophilic directional SRS can be further optimized by engineering the surface textures, tuning the lubricant viscosity, or using lubricant-infused polymers accordingly depending on specific applications (fig. S6). Our work not only demonstrates the first examples of applications using Wenzel state droplets but also shows the possibility of creating a hydrophilic coating with excellent droplet nucleation and water-repellent functions, which may contribute to a broad range of applications related to water and energy, such as antifouling for marine ships, dropwise condensation for power generation and desalination, and water harvesting in arid regions.

MATERIALS AND METHODS

Fabrication of nanotextured surface

The nanostructures were fabricated on a 100 mm <100> p-type silicon wafer with a thickness of 450 μm. We used a modified black silicon method (*37*), in which SF_6, C_4F_8, and O_2 with the flow rates of 300, 300, and 100 sccm (standard cubic centimeter per minute), respectively, were used to etch the plain silicon wafer and obtain uniform nanostructures. The nanotextured silicon wafer was cleaned using oxygen plasma. Subsequently, the sample was silanized using trimethylchlorosilane (Sigma-Aldrich). Afterward, lubricant such as Krytox 101 (viscosity of 17.4 cSt at 20°C; DuPont) or hydroxy-terminated PDMS (viscosity of 25 cSt at 25°C; Sigma-Aldrich) was coated on the silanized nanotextured silicon wafer using a spin coater (Laurell, model WS-650MZ-23NPP). We used a spin speed of 12,000 rpm to fully remove excess lubricant from the surface because the CA does not change when the spin speed is further increased (fig. S3D).

Dropwise condensation in ESEM

The lubricant-infused nanotextured surface was visualized using an ESEM (FEI Quanta 3D 200) by Peltier cooling to capture the surface morphology on an angled stage (tilted at 60°). The applied voltage was 20 kV, and the current was 2.1 nA for the operation of ESEM. The temperature was reduced to – 4.5° ± 0.5°C, and the pressure was set to 3.8 torr during the ESEM tests. All the images and videos were captured at the same pressure and temperature conditions.

Fog harvesting

A conventional ultrasonic humidifier (Crane EE-5301) was used to produce cool mist. The droplet size was 2 to 4 μm. All the surfaces were placed vertically, facing the mist, which flow toward the surface at a tilted angle of 45° ± 5°. The distance between the outlet of the mist and the vertical substrate was ~5 cm. To avoid the edge effect from the sample substrate, the mist was diverted onto the sample surface directly. The dripping water was collected by a clean beaker. The mass measurements of the collected water were performed using a high-resolution analytical balance (resolution = 0.1 mg; Mettler Toledo XP504 DeltaRange). The weight of the beaker before and after collection was measured as M_0 and M_a, respectively. The weight of the lubricated sample before and after collection was measured as M_{s0} and M_{sa},

respectively. The total mass of harvested fog in a given interval of time was $M_f = (M_{sa} + M_a) - (M_{s0} + M_0)$.

MD simulations

Two hundred twenty-four alkanethiol molecules have their sulfur atoms fixed in the *x*-*y* plane, as if they are bonded to a gold (111) surface, with lattice constant $a = 5\sqrt{2}$ (21.6 Å^2 per sulfur) following the study of Acharya *et al.* (*33*). The fully fluorinated chains have lattice constant $a = 5.9\sqrt{2}$ (30.1 Å^2 per sulfur) (*38*). Fully atomistic force field parameters were obtained from CGenFF (CHARMM General Force Field). The flexible SPC/E water model was used because it is one of the few water models with the correct liquid/vapor surface tension. The simulation cell was 300 Å high with a water vapor density of 2×10^{-4} molecules/Å^3; the upper 40 Å was thermostated at 450 K, and the initial water vapor temperature was set at 450 K; the alkanethiols were thermostated at 373 K to provide a "cool" surface following the study of Xu *et al.* (*32*). To mimic the hydroxy PDMS surface, three different randomly generated surfaces consisting of 80% $-CH_3$ and 20% –OH functionality of the alkanethiol molecules were constructed, each using a different seed for the random number generator so that the –OH functional sites were in different locations. This allows us to conduct three separate simulations to ensure that our results were not biased by any one choice of the functional group assignments. Detailed information about material design, lubrication and wetting characterization, and the MD simulations can be found in the Supplementary Materials.

SUPPLEMENTARY MATERIALS

Supplementary material for this article is available at http://advances.sciencemag.org/cgi/content/full/4/3/eaaq0919/DC1

section S1. Descriptions of movies S1 to S10
section S2. Design principle of surface structures
section S3. Wetting equations on liquid-infused surfaces
section S4. Design of SRS
section S5. Longevity of SRS
section S6. MD simulations for droplet nucleation
fig. S1. Design principle of the surface structures.
fig. S2. SEM images of nanotextures and SLIPS.
fig. S3. Wetting characteristics on liquid-infused slippery surfaces.
fig. S4. Wetting models of a water droplet on difference surfaces.
fig. S5. Design of directional SRS.
fig. S6. The effect of nanotextures on lubricant retention.
fig. S7. Nucleation on various functionalized surfaces.
table S1. CAs and thermal conductivities of different lubricants used in this study.
table S2. Time for most (70%) of the water vapor molecules to condense on the SAM surfaces.
Reference (*40*)

REFERENCES AND NOTES

1. W. Barthlott, C. Neinhuis, Purity of the sacred lotus, or escape from contamination in biological surfaces. *Planta* **202**, 1–8 (1997).
2. A. R. Parker, C. R. Lawrence, Water capture by a desert beetle. *Nature* **414**, 33–34 (2001).
3. S. Daniel, M. K. Chaudhury, J. C. Chen, Fast drop movements resulting from the phase change on a gradient surface. *Science* **291**, 633–636 (2001).
4. D. Quéré, Wetting and roughness. *Annu. Rev. Mater. Res.* **38**, 71–99 (2008).
5. T.-S. Wong, T. Sun, L. Feng, J. Aizenberg, Interfacial materials with special wettability. *MRS Bull.* **38**, 366–371 (2013).
6. A. Alizadeh, V. Bahadur, A. Kulkarni, M. Yamada, J. A. Ruud, Hydrophobic surfaces for control and enhancement of water phase transitions. *MRS Bull.* **38**, 407–411 (2013).
7. R. Xiao, N. Miljkovic, R. Enright, E. N. Wang, Immersion condensation on oil-infused heterogeneous surfaces for enhanced heat transfer. *Sci. Rep.* **3**, 1988 (2013).
8. S. Anand, A. T. Paxson, R. Dhiman, J. D. Smith, K. K. Varanasi, Enhanced condensation on lubricant-impregnated nanotextured surfaces. *ACS Nano* **6**, 10122–10129 (2012).
9. A. D. Khawaji, I. K. Kutubkhanah, J.-M. Wie, Advances in seawater desalination technologies. *Desalination* **221**, 47–69 (2008).
10. T. L. Liu, C.-J. Kim, Turning a surface superrepellent even to completely wetting liquids. *Science* **346**, 1096–1100 (2014).
11. A. Tuteja, W. Choi, M. Ma, J. M. Mabry, S. A. Mazzella, G. C. Rutledge, G. H. McKinley, R. E. Cohen, Designing superoleophobic surfaces. *Science* **318**, 1618–1622 (2007).
12. J. B. Boreyko, C.-H. Chen, Self-propelled dropwise condensate on superhydrophobic surfaces. *Phys. Rev. Lett.* **103**, 184501 (2009).
13. A. Lafuma, D. Quéré, Superhydrophobic states. *Nat. Mater.* **2**, 457–460 (2003).
14. N. Miljkovic, R. Enright, Y. Nam, K. Lopez, N. Dou, J. Sack, E. N. Wang, Jumping-droplet-enhanced condensation on scalable superhydrophobic nanostructured surfaces. *Nano Lett.* **13**, 179–187 (2013).
15. R. N. Wenzel, Resistance of solid surfaces to wetting by water. *Ind. Eng. Chem.* **28**, 988–994 (1936).
16. R. Wen, Q. Li, J. Wu, G. Wu, W. Wang, Y. Chen, X. Ma, D. Zhao, R. Yang, Hydrophobic copper nanowires for enhancing condensation heat transfer. *Nano Energy* **33**, 177–183 (2017).
17. T. Mouterde, G. Lehoucq, S. Xavier, A. Checco, C. T. Black, A. Rahman, T. Midavaine, C. Clanet, D. Quéré, Antifogging abilities of model nanotextures. *Nat. Mater.* **16**, 658–663 (2017).
18. T.-S. Wong, S. H. Kang, S. K. Y. Tang, E. J. Smythe, B. D. Hatton, A. Grinthal, J. Aizenberg, Bioinspired self-repairing slippery surfaces with pressure-stable omniphobicity. *Nature* **477**, 443–447 (2011).
19. A. Lafuma, D. Quéré, Slippery pre-suffused surfaces. *Europhys. Lett.* **96**, 56001 (2011).
20. K.-C. Park, P. Kim, A. Grinthal, N. He, D. Fox, J. C. Weaver, J. Aizenberg, Condensation on slippery asymmetric bumps. *Nature* **531**, 78–82 (2016).
21. X. Liu, P. Cheng, Dropwise condensation theory revisited Part II. Droplet nucleation density and condensation heat flux. *Int. J. Heat Mass Transf.* **83**, 842–849 (2015).
22. Y. Hou, M. Yu, X. Chen, Z. Wang, S. Yao, Recurrent filmwise and dropwise condensation on a beetle mimetic surface. *ACS Nano* **9**, 71–81 (2015).
23. H. Bai, L. Wang, J. Ju, R. Sun, Y. Zheng, L. Jiang, Efficient water collection on integrative bioinspired surfaces with star-shaped wettability patterns. *Adv. Mater.* **26**, 5025–5030 (2014).
24. P. Kim, M. J. Kreder, J. Alvarenga, J. Aizenberg, Hierarchical or not? Effect of the length scale and hierarchy of the surface roughness on omniphobicity of lubricant-infused substrates. *Nano Lett.* **13**, 1793–1799 (2013).
25. X. Dai, B. B. Stogin, S. Yang, T.-S. Wong, Slippery Wenzel state. *ACS Nano* **9**, 9260–9267 (2015).
26. F. Schellenberger, J. Xie, N. Encinas, A. Hardy, M. Klapper, P. Papadopoulos, H.-J. Butt, D. Vollmer, Direct observation of drops on slippery lubricant-infused surfaces. *Soft Matter* **11**, 7617–7626 (2015).
27. D. Wu, J.-N. Wang, S.-Z. Wu, Q.-D. Chen, S. Zhao, H. Zhang, H.-B. Sun, L. Jiang, Three-level biomimetic rice-leaf surfaces with controllable anisotropic sliding. *Adv. Funct. Mater.* **21**, 2927–2932 (2011).
28. T. Guo, P. Che, L. Heng, L. Fan, L. Jiang, Anisotropic slippery surfaces: Electric-driven smart control of a drop's slide. *Adv. Mater.* **28**, 6999–7007 (2016).
29. C. G. L. Furmidge, Studies at phase interfaces. I. The sliding of liquid drops on solid surfaces and a theory for spray retention. *J. Colloid Sci.* **17**, 309–324 (1962).
30. J. B. Boreyko, G. Polizos, P. G. Datskos, S. A. Sarles, C. P. Collier, Air-stable droplet interface bilayers on oil-infused surfaces. *Proc. Natl. Acad. Sci. U.S.A.* **111**, 7588–7593 (2014).
31. X. Qu, J. B. Boreyko, F. Liu, R. L. Agapov, N. V. Lavrik, S. T. Retterer, J. J. Feng, C. P. Collier, C.-H. Chen, Self-propelled sweeping removal of dropwise condensate. *Appl. Phys. Lett.* **106**, 221601 (2015).
32. W. Xu, Z. Lan, B. L. Peng, R. F. Wen, X. H. Ma, Effect of surface free energies on the heterogeneous nucleation of water droplet: A molecular dynamics simulation approach. *J. Chem. Phys.* **142**, 054701 (2015).
33. H. Acharya, S. Vembanur, S. N. Jamadagni, S. Garde, Mapping hydrophobicity at the nanoscale: Applications to heterogeneous surfaces and proteins. *Faraday Discuss.* **146**, 353–365 (2010).
34. M. Szöri, D. J. Tobias, M. Roeselová, Microscopic wetting of mixed self-assembled monolayers: A molecular dynamics study. *J. Phys. Chem. B* **113**, 4161–4169 (2009).
35. D. Daniel, M. N. Mankin, R. A. Belisle, T.-S. Wong, J. Aizenberg, Lubricant-infused micro/nano-structured surfaces with tunable dynamic omniphobicity at high temperatures. *Appl. Phys. Lett.* **102**, 231603 (2013).
36. J. Ju, H. Bai, Y. Zheng, T. Zhao, R. Fang, L. Jiang, A multi-structural and multi-functional integrated fog collection system in cactus. *Nat. Commun.* **3**, 1247 (2012).
37. H. Jansen, M. de Boer, R. Legtenberg, M. Elwenspoek, The black silicon method: A universal method for determining the parameter setting of a fluorine-based reactive ion etcher in deep silicon trench etching with profile control. *J. Micromech. Microeng.* **5**, 115–120 (1995).
38. V. H. Dalvi, P. J. Rossky, Molecular origins of fluorocarbon hydrophobicity. *Proc. Natl. Acad. Sci. U.S.A.* **107**, 13603–13607 (2010).

39. G. D. Bixler, B. Bhushan, Rice- and butterfly-wing effect inspired self-cleaning and low drag micro/nanopatterned surfaces in water, oil, and air flow. *Nanoscale* **6**, 76–96 (2014).
40. C. Zhu, Y. Gao, H. Li, S. Meng, L. Li, J. S. Francisco, X. C. Zeng, Characterizing hydrophobicity of amino acid side chains in a protein environment via measuring contact angle of a water nanodroplet on planar peptide network. *Proc. Natl. Acad. Sci. U.S.A.* **113**, 12946–12951 (2016).

Acknowledgments
Funding: We acknowledge funding support by NSF CAREER (Faculty Early Career Development Program) Award 1351462 (cross-species materials and wetting science), Advanced Research Projects Agency-Energy Award DE-AR0000326 (condensation heat transfer), Office of Naval Research Multidisciplinary University Research Initiatives Award N00014-12-1-0875 (materials fabrication), Wormley Family Early Career Professorship, and the Humanitarian Materials Initiative Award sponsored by Covestro LLC and the Materials Research Institute at The Pennsylvania State University. B.B.S. acknowledges support from the NSF Graduate Research Fellowship (grant no. DGE1255832). Part of the work was conducted at the Penn State node of the NSF-funded National Nanotechnology of Infrastructure Network. **Author contributions:** X.D. and T.-S.W. conceived the research. X.D., S.Y., and T.-S.W. designed the experiments. X.D. and N.S. performed materials fabrication and characterizations. S.O.N. performed MD simulations. X.D. and B.B.S. conducted data analysis. X.D. and J.W. performed wetting characterizations. X.D., B.B.S., and T.-S.W. wrote the paper. All authors contributed to paper revision. **Competing interests:** X.D., N.S., B.B.S., J.W., and T.-S.W. are inventors on a pending patent application filed by the Penn State Research Foundation (application no. PCT/US2016/028959, filed on 22 April 2016). The authors declare that they have no other competing interests. **Data and materials availability:** All data needed to evaluate the conclusions in the paper are present in the paper and/or the Supplementary Materials. Additional data related to this paper may be requested from the authors.

Submitted 29 September 2017
Accepted 12 February 2018
Published 30 March 2018
10.1126/sciadv.aaq0919

Citation: X. Dai, N. Sun, S. O. Nielsen, B. B. Stogin, J. Wang, S. Yang, T.-S. Wong, Hydrophilic directional slippery rough surfaces for water harvesting. *Sci. Adv.* **4**, eaaq0919 (2018).

Hydrophilic directional slippery rough surfaces for water harvesting

Xianming Dai, Nan Sun, Steven O. Nielsen, Birgitt Boschitsch Stogin, Jing Wang, Shikuan Yang and Tak-Sing Wong

Sci Adv **4** (3), eaaq0919.
DOI: 10.1126/sciadv.aaq0919